Coupled aggregation and sedimentation processes: The sticking probability effect

G. Odriozola,[1] R. Leone,[1] A. Schmitt,[2] A. Moncho-Jordá,[2] and R. Hidalgo-Álvarez[2,*]
[1]*Departamento de Química Física y Matemática, Facultad de Química, Universidad de la República, 11800 Montevideo, Uruguay*
[2]*Departamento de Física Aplicada, Universidad de Granada, Campus de Fuentenueva, E-18071 Granada, Spain*
(Received 7 July 2002; revised manuscript received 20 December 2002; published 18 March 2003)

The influence of the sticking probability P and the drift velocity on kinetics and structure formation arising in coupled aggregation and sedimentation processes was studied by means of simulations. For this purpose, a large prism with no periodical conditions for the sedimentation direction was considered allowing for sediment formation at the prism base. The time evolution of the cluster size distribution (CSD) and weight-average cluster size (n_w) were determined in three different regions of the prism. The cluster morphology and the sediment structure were also analyzed. We found that the coupled aggregation and sedimentation processes in the bulk are governed by P for short times, and controlled by the Péclet number Pe for long times. In the lower part of the reaction volume, where the sediment grows, the local n_w grows at sufficiently large times analytically with an exponent of four. This behavior seems to be independent of Pe and P. The obtained results are in good agreement with the experimental data reported by C. Allain, M. Cloitre, and M. Wafra [Phys. Rev. Lett. **74**, 1478 (1995)] and support the idea of a possible internal cluster rearrangement for the experiments. Finally, we discuss how the scale dependent fractal character of the sediment is related to the different stages of the aggregation process.

DOI: 10.1103/PhysRevE.67.031401 PACS number(s): 82.70.Dd, 61.43.Hv, 02.50.−r

I. INTRODUCTION

Due to its presence in many natural and human-made processes, aggregation and sedimentation phenomena arising in mesoscopic systems have attracted a great deal of interest for pure science and industrial applications [2,3]. Although they are frequently found simultaneously and show a cooperative behavior, it was not until the last few years that scientists have started to study them as a whole. The reason for that may lie in the complexity of the equations that govern the overall process. Hence, it is not surprising that simulations have turned an important tool for understanding and predicting the behavior of such coupled phenomena.

In the literature, pure irreversible aggregation processes, i.e., those where neither sedimentation effects nor cluster breakup take place, have been classified according to the cluster sticking probability [4–6]. Freely diffusing particles which always aggregate once they collide are doing so in the so-called diffusion-limited cluster aggregation (DLCA) regime [7,8]. The regime in which a large number of collisions is needed before a new aggregate is formed, is known as reaction-limited cluster aggregation (RLCA) [9,10]. The first regime is characterized by a fast evolving cluster-size distribution (CSD) and a cluster fractal dimension d_f close to 1.75 [11–14]. The latter regime develops much slower in time and is characterized by $d_f=2.1$ [15,16].

To the best of our knowledge, all so far reported simulations of coupled aggregation and sedimentation processes have been performed imposing DLCA conditions [17–20]. Doing so, Gonzalez found a shift of d_f to higher values, which was in good agreement with the experimental results reported by Allain, Cloitre, and Wafra [1,21,22]. He also predicts that the critical mass concentration required for gelation increases for increasing settling effects. In a former paper, the authors show how the time evolution of the CSD depends on the position inside the reaction volume and determine how the sediment grows at the bottom [20].

In this paper, we lift the imposed DLCA restriction and study the influence of P on coupled aggregation and sedimentation processes by means of simulations. For this purpose, a large prism with no periodic boundary conditions for the sedimentation direction was considered, and P as well as Pe were introduced as free parameters.

II. SIMULATIONS

The simulations were performed off-lattice and on a square section prism of side L and height H. Inside the prism volume, N_0 identical particles of radius a were randomly placed avoiding particle overlap. Two contributions to the particle movement were considered: a random Brownian motion and a vertical sedimentation velocity. The time step was defined by $t_0=l_B^2/6D_1$, where $D_1 = k_BT/(6\pi\eta a)$ is the monomer diffusion coefficient, k_BT is the thermal energy, η is the solvent viscosity, and l_B is the Brownian step length. The monomeric particles are always moved a fixed distance l_B in a random direction plus an additional vertical Stokes contribution due to sedimentation. The step length for the latter contribution is given by $l_S=v_St_0=l_B^2\mathrm{Pe}/6a$, where $v_S=2(\rho-\rho_0)ga^2/(9\eta)$ is the Stokes velocity for the monomeric particles, ρ is the particle mass density, ρ_0 is the fluid density, g is the gravitational acceleration, and $\mathrm{Pe}=4\pi a^4(\rho-\rho_0)g/3k_BT$ is the Péclet number. For further details see Ref. [20].

When a collision takes place, a random number ξ uniformly distributed in [0,1] is generated and compared with the given P. The cluster collision is considered effective only when $\xi<P$ is verified. Periodic boundary conditions were imposed for the horizontal directions, x and y. In the settling

*Email address: rhidalgo@ugr.es

direction, cluster movement was restricted to the prism size. This means that settling will give rise to sediment formation at the prism base. We arbitrarily divided the system in three equally sized and mutually excluded regions (an upper, a middle and a lower region). For each one, the weight-average cluster size is defined as $n_w|_h = \Sigma_i i^2 n_i|_h / \Sigma_i i n_i|_h$, where n_i is the number of i-sized clusters and h, which may be equal to top, middle, or bottom, stands for the corresponding region in the reaction volume.

The cluster anisotropy and cluster orientation, as defined in Ref. [1], are calculated for comparing the simulation results with the data reported by Allain, Cloitre, and Wafra. The d_f is determined for each of the three defined regions by means of the relationship $r_g = a i^{1/d_f}$, where r_g is the cluster radius of gyration [14,23]. All geometric quantities such as orientations, anisotropies and d_f are averaged by considering only clusters formed by more than 20 constituting particles. Finally, a fractal dimension analysis is also performed for the sediment. This is done just as explained in Ref. [20].

The parameters employed for the simulations are as follows: monomer radius $a = 315$ nm, Brownian step length $l_B = a/2$, prism height $H = 10\,000a$, a prism side length $L = 250a$ and particle volume fraction $\phi = 6.7 \times 10^{-5}$ (i.e. $N_0 = 10000$). The particles were considered to be dispersed in water at 20°C.

III. RESULTS

A. Kinetic aspects

After having discussed the kinetics of a fast aggregating system in Ref. [20], we now focus our attention on identical systems with a substantially lower P. As expected, the CSD of this type of systems develops initially very slowly in time and maintains an almost constant monomer concentration. Even the n_w increases only very little. This behavior is very similar to that observed for pure RLCA. For longer times, however, mass starts being transferred from the upper regions to the prism base. Hence, only smaller aggregates can be formed in the upper regions. Consequently, for the upper regions, n_w peaks at smaller values and longer times than for $P = 1$.

The lower region, however, behaves very differently. After a sufficiently long time, the cluster concentration increases significantly due to cluster uptake from the upper regions. Hence, the collision frequency rises and starts to compensate the small P. This effect is very pronounced at the prism base where all incoming clusters accumulate and are forced to move almost restricted to two dimensions. Hence, two-dimensional aggregation is favored and larger clusters form even at relatively short times, well before they are formed in the bulk. Consequently, the time evolution of the larger cluster concentrations shows a clear double peak. This is seen in Fig. 1. Evidently, n_w starts to increase steeply as soon as the first peaks start to develop, indicating the beginning of a sol-gel transition [22,24].

The time evolution of n_w for $P = 1$ and 0.01, and for Pe $= 1$, 0.1, 0.01, and 0.001 are shown in Fig. 2. In this figure, only the lower regions are included. The upper region is not shown, since its behavior is very similar to that found for the middle region. The only important difference is that the maxima of n_w in the center of the reaction volume reach higher values than in the upper region. For all regions, the data seem to follow a single master curve at short times. The shape of this master curve depends only on P. For $P = 1$ it is very similar to that usually obtained for pure DLCA processes, while for $P = 0.01$ it exhibits a typical RLCA behavior. This means that, for short times, the time evolution of the CSD is mainly controlled by cluster aggregation and sedimentation effects are not yet important. At longer times, the different curves abandon this common behavior the earlier the higher Pe becomes. In the upper regions, this separation occurs when n_w starts to diminish. Afterwards, they also seem to follow a kind of a master curve. In this case, however, only curves with the same Pe show a similar behavior independently of P. This implies that, at longer times, the coupled aggregation-sedimentation processes are mainly sedimentation controlled. Moreover, all curves diminish with a constant slope of approximately -2. For the lower region, the curves separate from the short time master curves developing a steep increase in time. Please note that, also in this case, the curves seem to have a common slope, but now with an exponent of approximately four.

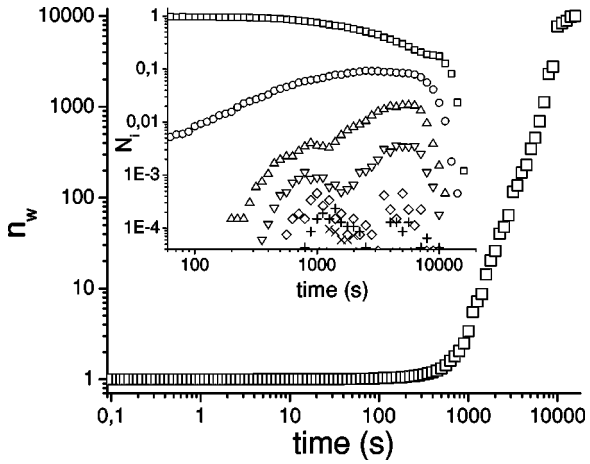

FIG. 1. Time evolution of n_w, for Pe $= 0.1$ and $P = 0.01$, and for h equal to *bottom*. The upper left inset shows the corresponding normalized CSD grouped in logarithmically spaced intervals [(□), monomers; (○), 2- and 3-mers; (△), 4- to 8-mers; (▽), 9 to 18-mers; (◇), 19- to 38-mers; and (+), 39- to 88-mers].

B. Morphological aspects

1. Anisotropy and orientation

The cluster anisotropy and orientation were calculated for the sake of comparison with the experimental data reported by Allain, Cloitre, and Wafra [1,21,22]. The obtained results are summarized in Table I for the lower regions and all considered Pe and P. Some data could not be obtained due to the small number of larger clusters formed under the corresponding simulation conditions. The data obtained for the upper region do not differ very much from those obtained for the middle region, and so are not shown. It should be noted that the average orientation is always close to zero. In order to

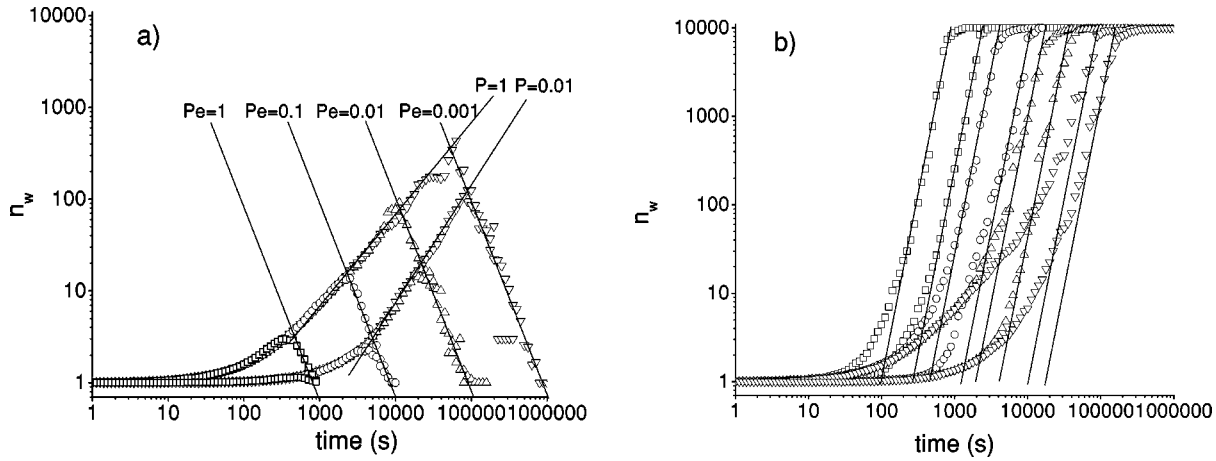

FIG. 2. Time evolution of n_w for different Pe and P, for the middle (a) and lower (b) regions of the system. The symbols □, ○, △, and ▽ correspond to Pe=1, 0.1, 0.01 and 0.001, respectively. For each Pe, two curves are plotted. The faster evolving curves correspond to $P=1$ and the others to $P=0.01$.

interpret this finding correctly it is important to pay attention to the corresponding standard deviations. For the upper regions, these values are practically constant and very close to 52°, which is just the standard deviation for a constant distribution in the interval $[-90°,90°]$. Hence, we may conclude that the cluster orientation does not take a preferential value. This general result is in very good agreement with the experimental observations reported by Allain, Cloitre, and Wafra [1,21,22]. For the lower region, however, the standard deviations diminish for increasing Pe and, to a smaller extent, also for decreasing P. A value as low as 7.0 is obtained for Pe=1 and $P=0.01$. This means that the clusters tend to be horizontally orientated, i.e., the longer axes of the clusters aligns parallel to the prism base.

From the anisotropy data shown in Table I, one observes that the obtained values stray around 1.9 in the middle region. The experimental value reported by Allain, Cloitre, and Wafra is, however, 1.47 ± 0.02 [1] which means that the simulated clusters are much longer than real aggregates. This indicates that rearrangement processes occur inside real aggregates, as was suggested by Allain. Furthermore, we did not find any correlation between the anisotropy and the cluster size, which is also in good agreement with the experimental results. Due to the presence of the prism base, the anisotropy in the lower region also differs from the values obtained for the bulk. Here, the anisotropy increases for increasing Pe and, to a smaller extend, for decreasing P. Please note that for Pe=1 and $P=0.01$, the anisotropy rises up to 4.88. This implies that the sediment presents two long principal sides, parallel to the prism base, but a very short minor side, perpendicular to the prism base.

TABLE I. Orientation and anisotropy as a function Pe and P for the lower regions. The error values for the orientation and for the anisotropy correspond to the standard deviation of the population and to the standard deviation of the average, respectively.

		Orientation		Anisotropy	
Pe	P	Middle	Bottom	Middle	Bottom
1	1		-0.5 ± 27.2		2.26 ± 0.12
1	0.1		-0.5 ± 11.9		3.51 ± 0.09
1	0.01		-2.2 ± 7.0		4.88 ± 0.04
0.1	1	-10.3 ± 44.3	-1.3 ± 42.3	1.94 ± 0.05	1.95 ± 0.03
0.1	0.1	8.2 ± 40.9	5.7 ± 42.3	1.75 ± 0.08	2.31 ± 0.06
0.1	0.01		4.8 ± 26.4		2.03 ± 0.05
0.01	1	-4.2 ± 50.2	-4.2 ± 53.4	1.91 ± 0.03	1.84 ± 0.03
0.01	0.1	-9.1 ± 53.6	0.0 ± 53.4	1.75 ± 0.03	1.78 ± 0.03
0.01	0.01	0.4 ± 50.2	-3.6 ± 45.5	1.82 ± 0.06	1.97 ± 0.04
0.001	1	6.6 ± 54.4	-0.4 ± 52.7	1.75 ± 0.03	1.83 ± 0.03
0.001	0.1	7.0 ± 50.3	2.1 ± 49.2	1.78 ± 0.03	1.78 ± 0.03
0.001	0.01	2.1 ± 49.0	-0.2 ± 52.7	1.73 ± 0.03	1.70 ± 0.03

2. Cluster fractal dimensions

The d_f obtained for the three regions and all simulation conditions are summarized in Table II. For the upper regions and for Pe=0.001 and $P=1$, the values 1.76 and 1.79 are found. They are very close to generally accepted value of

TABLE II. $d_f|_h$ as a function of Pe and P. As usual, h refers to the top, the middle, and the bottom regions.

Pe	P	$d_f\|_{top}$	$d_f\|_{middle}$	$d_f\|_{bottom}$
1	1			1.65 ± 0.07
1	0.1			1.67 ± 0.05
1	0.01			1.62 ± 0.04
0.1	1	1.81 ± 0.07	1.84 ± 0.06	1.81 ± 0.06
0.1	0.1		1.88 ± 0.06	1.85 ± 0.05
0.1	0.01			1.84 ± 0.05
0.01	1	1.85 ± 0.05	1.84 ± 0.06	1.83 ± 0.04
0.01	0.1	1.86 ± 0.06	1.83 ± 0.04	1.86 ± 0.05
0.01	0.01	1.95 ± 0.05	2.15 ± 0.07	2.05 ± 0.03
0.001	1	1.76 ± 0.04	1.79 ± 0.05	1.79 ± 0.03
0.001	0.1	1.83 ± 0.05	1.85 ± 0.05	1.89 ± 0.04
0.001	0.01	1.90 ± 0.04	1.93 ± 0.05	2.03 ± 0.03

TABLE III. $d_f|_m$ as a function of Pe and P. The subscript index m refers to the intrasediment distance interval used for the fit. The considered intervals were $r/a=[3,10]$, $[30,50]$, and $[70,100]$ for $m=1$, 2, and 3, respectively.

Pe	P	$d_f\|_1$	$d_f\|_2$	$d_f\|_3$
1	1	1.98 ± 0.04	1.85 ± 0.05	1.62 ± 0.05
1	0.1	2.06 ± 0.05	1.77 ± 0.05	1.59 ± 0.05
1	0.01	2.20 ± 0.04	1.59 ± 0.04	1.57 ± 0.05
0.1	1	1.87 ± 0.04	1.98 ± 0.05	1.60 ± 0.05
0.1	0.1	2.03 ± 0.05	1.85 ± 0.05	1.53 ± 0.06
0.1	0.01	2.26 ± 0.05	1.60 ± 0.05	1.51 ± 0.05
0.01	1	1.80 ± 0.04	2.03 ± 0.05	1.97 ± 0.06
0.01	0.1	1.89 ± 0.05	2.05 ± 0.04	1.57 ± 0.05
0.01	0.01	2.07 ± 0.04	1.83 ± 0.04	1.54 ± 0.05
0.001	1	1.79 ± 0.05	1.94 ± 0.05	2.06 ± 0.05
0.001	0.1	1.87 ± 0.04	1.96 ± 0.04	1.96 ± 0.05
0.001	0.01	1.99 ± 0.04	2.05 ± 0.05	1.69 ± 0.05

1.75 ± 0.05 for pure DLCA. Either an increasing Pe or a decreasing P leads to an increase of d_f. This effect, however, is more pronounced for changes in P. The influence of P on d_f is well known [25]. Usually, more compact structures are formed which are characterized by $d_f=2.1$ [9,11,26]. The influence of Pe was recently studied by González [17–19]. He found that an increasing Pe also leads to higher d_f. The reason for this is that a higher Pe increases the difference between the settling velocity of large and small clusters. Hence, the larger clusters sweep an even larger volume and so, collide more often with smaller aggregates. Since the smaller clusters penetrate easily into the open structure of the larger aggregates, an increasing d_f is expected. Please note that our data are in good agreement with this statement made by González. The d_f values in the middle region tend to be larger than those observed in the upper region. This is, of course, due to the fact that only relatively small clusters are achieved in the upper region.

In the lower region, the two-dimensionally restricted sediment growth process has an influence on the cluster structure only when cluster formation in the bulk is not important, i.e., for fast settling and slowly aggregating particles. In this case, one expects d_f to tend towards the values typically observed for two dimensional aggregation (1.45 for 2D-DLCA and 1.55 for 2D-RLCA [27]). As can be seen in Table II, our data confirm this hypothesis since d_f decreases for increasing Pe and for decreasing P. For systems which aggregate mainly in the bulk, d_f is very similar to the values obtained for the upper regions. In the following section we give a more detailed analysis of the sediment, excluding the dispersed particles in the bulk of the lower region.

3. Sediment fractal dimensions

The d_f obtained from the multifractal analysis of the sediment are shown in Table III. We start the discussion focusing on the $d_f|_1$ values. These values correspond to relatively short intrasediment distances and hence, are related to the aggregation of the smallest clusters. Since these clusters are mainly produced in the bulk before they arrive at the prism bottom, it is not surprising that the $d_f|_1$ reach values closed to those obtained for the clusters formed in the upper regions.

$d_f|_2$ was calculated for intrasediment distances between $r/a=30$ and $r/a=50$. For small Pe, the obtained values tend to be somewhat larger than $d_f|_1$. Here, the settling velocity is still so small that the aggregates arriving at the prism bottom are larger than the considered length interval. Hence, the sediment builds up starting from larger clusters formed in the bulk. As explained before, the d_f of settling clusters tends to increase with cluster-size and so, higher d_f are achieved at longer intrasediment distances. This effect should be even more pronounced for larger Pe. Nevertheless, the opposite behavior is found since $d_f|_2$ decreases for increasing Pe. Moreover, the expected dependency on P is also reversed obtaining a smaller d_f for decreasing P. As a matter of fact, the extremely low value of 1.59 was obtained for $P=0.01$ and $\mathrm{Pe}=1$. This can be explained as follows: For high Pe, the clusters settle so fast that they have not enough time to aggregate before they arrive at the prism base. For small P, something similar happens since the CSD evolves so slowly that even the smaller aggregates have enough time to settle without growing too much. In both cases, the overall effect is that only relatively small clusters arrive at the prism base. Hence, the larger aggregates and the sediment are mainly formed by two-dimensional aggregation of smaller clusters. This implies that d_f even at relatively short length scales tends towards smaller values.

$d_f|_3$, defined for even larger intrasediment distances, confirm this hypothesis. As can be seen in Table III, the expected tendency is now observed also for smaller Pe and larger P. Moreover, d_f seems to have a limiting value around 1.55. This value is commonly reported for $2D$-RLCA and so, indicates quite clearly that the sediment is formed by two-dimensional diffusion of smaller cluster at the prism bottom. On the other hand, sediments that are not mainly formed at the prism base keep a high fractal dimension.

IV. CONCLUSIONS

As expected, decreasing P leads to a slower time evolution of the CSD in the upper regions of the system and causes the n_w to peak later at lower values. For the lower region, however, it was shown that aggregation at the prism base becomes more important for decreasing P and thus, compensates the slow time evolution in the bulk. Hence, n_w increases as a steep function of time indicating a sol-gel transition. Moreover, the n_w reach at sufficiently large times a slope of four, which seems to be independent of Pe and P. At short times and for the bulk, the time evolution of n_w follows a single master curve which depends only on P and seems to be independent of the Pe. Furthermore, curves with the same Pe also show a very similar behavior among themselves. This allows us to conclude that coupled aggregation and sedimentation processes taking place in the bulk are at short times governed by P and at long times controlled by Pe.

On one hand, the cluster anisotropy of the aggregates pro-

duced in the bulk was found to be larger than the experimental values reported by Allain, Cloitre, and Wafra [1]. This supports their assumption of possible particle rearrangement processes inside the clusters. On the other hand, no preferential orientation of the clusters was observed, what is in good agreement with their data. The fractal dimensions of the clusters formed in the bulk were found to behave as expected, i.e., to increase for increasing Pe and decreasing P.

The cluster morphology in the lower region was affected by the sediment formation. This influence was shown to be very important when the system conditions caused the aggregation process to be accomplished mostly at the prism base. In this case, the sediment orientation was essentially parallel to the prism base, and the sediment shows a higher anisotropy and a clear multifractal character. Furthermore, it was shown how this multifractal behavior is related to the almost two dimensional restricted aggregation of the clusters that arrive at the prism base and collide to form the sediment.

ACKNOWLEDGMENTS

This work was supported by the Spanish Ministerio de Ciencia y Tecnología, Plan Nacional de Investigación, Desarrollo e Innovación Tecnológica ($I+D+I$) (Project No. MAT2000-1550-C03-01). G.O. is grateful for financial support granted by the Uruguayan CSIC (Ref. 004010-001187-01) and PEDECIBA.

[1] C. Allain, M. Cloitre, and M. Wafra, Phys. Rev. Lett. **74**, 1478 (1995).
[2] R.J. Hunter, *Foundations of Colloid Science* (Clarendon Press, Oxford, 1987).
[3] J. Lyklema, *Fundamentals of Interface and Colloid Science. Volume I: Fundamentals* (Academic Press, London, 1991).
[4] P. Meakin and F. Family, Phys. Rev. A **38**, 2110 (1988).
[5] M. Thorn and M. Seesselberg, Phys. Rev. Lett. **72**, 3622 (1994).
[6] G. Odriozola, A. Moncho-Jordá, A. Schmitt, J. Callejas-Fernández, R. Martínez-García, and R. Hidalgo-Álvarez, Europhys. Lett. **53**, 797 (2001).
[7] T. Vicsek, P. Meakin, and F. Family, Phys. Rev. A **32**, 1122 (1985).
[8] M.Y. Lin, H.M. Lindsay, D.A. Weitz, R. Klein, R.C. Ball, and P. Meakin, J. Phys.: Condens. Matter **2**, 3093 (1990).
[9] P. Meakin and F. Family, Phys. Rev. A **36**, 5498 (1987).
[10] M.Y. Lin, H.M. Lindsay, D.A. Weitz, R.C. Ball, R. Klein, and P. Meakin, Phys. Rev. A **41**, 2005 (1990).
[11] D.A. Weitz and M. Oliveria, Phys. Rev. Lett. **52**, 1433 (1984).
[12] F. Family and D.P. Landau, *Kinetics of Aggregation and Gelation* (North-Holland, Amsterdam, 1984).
[13] M. Kolb, Phys. Rev. Lett. **53**, 1653 (1984).
[14] P. Meakin, Phys. Rev. B **29**, 2930 (1984).
[15] F. Family, P. Meakin, and T. Vicsek, J. Chem. Phys. **83**, 4144 (1985).
[16] M.L. Broide and R.J. Cohen, Phys. Rev. Lett. **64**, 2026 (1990).
[17] A.E. González and F. Leyvraz, in *Statistical Mechanics in Physics and Biology*, edited by D. Wirtz and T.C. Halsey, Mater. Res. Soc. Symp. Proc. 463 (Materials Research Society, Pittsburgh, 1997).
[18] A.E. González, Phys. Rev. Lett. **86**, 1243 (2001).
[19] A.E. González, J. Phys.: Condens. Matter **14**, 2335 (2002).
[20] R. Leone, G. Odriozola, L. Mussio, A. Schmitt, and R. Hidalgo-Álvarez, Eur. Phys. J. E **7**, 153 (2002).
[21] C. Allain, M. Cloitre, and F. Parisse, J. Colloid Interface Sci. **179**, 411 (1996).
[22] D. Senis, L. Gorre-Talini, and C. Allain, Eur. Phys. J. E **4**, 59 (2001).
[23] P. Meakin, *Fractals, Scaling and Growth Far from Equilibrium* (Springer, Cambridge, 1998).
[24] S.B. Grant, J. Ha Kim, and C. Poor, J. Colloid Interface Sci. **238**, 238 (2001).
[25] G.C. Bushell, Y.D. Yan, D. Woodfield, J. Raper, and R. Amal, Adv. Colloid Interface Sci. **95**, 1 (2002).
[26] A.E. González, Phys. Rev. Lett. **71**, 2248 (1993).
[27] R. Jullien and M. Kolb, J. Phys. A **17**, L639 (1984).